

See discussions, stats, and author profiles for this publication at: <https://www.researchgate.net/publication/282238004>

Design of Ion-Containing Polymer-Grafted Nanoparticles for Conductive Membranes

ARTICLE *in* MACROMOLECULES · JULY 2015

Impact Factor: 5.8 · DOI: 10.1021/acs.macromol.5b00758

READS

26

3 AUTHORS, INCLUDING:



Tsengming Chou

Stevens Institute of Technology

32 PUBLICATIONS 384 CITATIONS

[SEE PROFILE](#)



Pinar Akcora

Stevens Institute of Technology

50 PUBLICATIONS 612 CITATIONS

[SEE PROFILE](#)

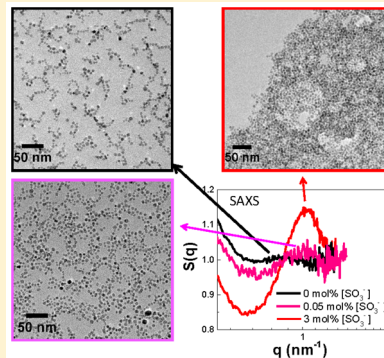
Design of Ion-Containing Polymer-Grafted Nanoparticles for Conductive Membranes

Yang Jiao, Tsengming Chou, and Pinar Akcora*

Department of Chemical Engineering & Materials Science, Stevens Institute of Technology, Hoboken, New Jersey 07030, United States

Supporting Information

ABSTRACT: While sulfonated polymers are commonly used in membranes for fuel cells and water filtration applications, challenges of controlling ionic aggregation and understanding morphology effects on conductivity and transport still remain. In this work, we investigate the aggregation of copolymer-grafted nanoparticles that are designed to form conductive structures with low sulfonation amounts of chains. We demonstrate that long grafts of polystyrene chains with sulfonated end groups form side-by-side aggregated strings and retain their structures in ionic liquid, 1-hexyl-3-methylimidazolium bis(trifluoromethylsulfonyl)imide, [HMIM][TFSI]. Transmission electron tomography results revealed that these aggregates are monolayers of particles at low sulfonations and planar-like networks at 3 mol % sulfonation in the ionic liquid. Organization of magnetic nanoparticles with the polymer grafting approach is shown, for the first time, to enhance conductivity upon incorporation of an ionic liquid.



INTRODUCTION

Hybrid electrolytes have been of interest to many researchers as they have potential applications in electroactive actuators, energetic devices such as batteries, fuel cells, and filtration membranes.^{1–5} Inclusion of fillers to polymer electrolytes improves their mechanical and transport behavior. Surface-modified charged fillers or polymers are designed to couple both mechanical and conductive properties. For example, functionalized silica particles with anions or ionic liquid polymer brushes are shown to behave as single-ion conductors.^{5–10} Moreover, densely grafted nanofillers with poly(ethylene glycol) oligomers and poly(poly(ethylene glycol)) methyl ether methacrylate (P(PEGMA)) based block copolymer electrolytes exhibit enhanced mechanical modulus and ionic conductivity.^{11,12} With colloidal crystals of hybrid silica nanoparticles, ion conductivity is enhanced with the assembly of particles decorated with ionic liquid type polymer brushes and form network channels within connected brush domains.¹³ This reported 3-dimensional assembly of colloidal crystals is clearly different than hybrid electrolytes since conductive channels are created within ordered particles.

In this work, self-assembly of noncrystalline grafted nanoparticles is utilized to form connected grafted-polymer domains to attain transport properties. It has been demonstrated that polymer-grafted nanoparticles self-assemble into anisotropic structures due to microphase separation between the particle core and grafted chains.^{14–16} Theoretical and simulation works have rationalized the experimental findings of anisotropic assembly of particles.¹⁷ Many experimental and theoretical works have studied the effect of several factors such as particle size, grafting density, graft length, polydispersity, and chemical heterogeneity as in block copolymers.^{18–26} In our recent work,

anisotropic particle assembly has been achieved in bulk films using magnetite particles grafted with long polymer chains at low grafting densities, where the inorganic core and organic chains are both hydrophobic.^{27–29} While directing magnetic nanoparticles within block copolymers has been studied in past works,^{30,31} our main interest in working with polymer-grafted superparamagnetic nanoparticles is to show that by mediating the interactions between particles, competition between enthalpic and entropic interactions arises and strings can form. This assembly is not due to dislike between core and polymer chains, but rather due to additional interactions between very small particles (smaller than 10 nm in diameter), which has been driven by competition between the short-range attractive dipolar and van der Waals forces and long-range repulsive forces. Thus, with ~8 nm magnetite particles grafted with long chains (100 kg/mol polystyrene with 0.013 chains/nm² graft density), strings are obtained in both solvent-free condition (i.e., in polymer matrix) and in the vicinity of solvent (i.e., good solvent for grafted chains and particles). In our previous work, we reported that ion-containing polymer-grafted nanoparticles form highly ordered chain-like structures below 3 mol % sulfonation in bulk at two particle loadings (5 and 15 wt %).³² It is shown that the miscibility of grafts with free matrix chains may inhibit ions to aggregate into clusters. For example, sulfonated long grafted chains form compact aggregates of strings when they are immiscible with long free chains.³²

One-component system of polymer-grafted nanoparticles avoids the issues associated with the miscibility between grafted

Received: April 11, 2015

Revised: May 10, 2015

Published: July 10, 2015

and matrix chains and also maximizes the volume fractions of particles which helps particles to organize into continuous network (bundles of wires) as also suggested by a recent simulation work.²⁰ Our strategy of grafting polymers on magnetite nanoparticles is utilized here to create conductive self-assembled particle nanostructures containing ionic chain ends without any matrix polymer.^{14,27} String forming particles are functionalized with hydrophilic units of sulfonated polystyrene to observe the effect of these end units on the assembly of particles and also to understand how particles aggregate in a good proton mediator such as ionic liquids, which is a selective solvent for the hydrophilic domain. The goal of this work is therefore to demonstrate that ionic interactions between polystyrene-*b*-polystyrenesulfonate (PS-*b*-PSS) copolymer-grafted magnetite (Fe_3O_4) nanoparticles can induce the aggregation of strings into monolayer structures as opposed to forming spherical clusters observed in sulfonated polymers. In addition, the segregation between hydrophobic and hydrophilic domains enables the effective swelling of the hydrophilic units with ionic liquid.

Here, we explore the organization of lightly sulfonated polymer grafted nanoparticles in transmission electron microscopy (TEM) and small-angle X-ray scattering (SAXS) experiments. Styrenesulfonates (SS), neutralized with trioctylammonium (TOA), are attached to free ends of tethered polystyrene (PS) chains via thiol–ene click reactions to prepare copolymer-grafted magnetite nanoparticles. Particle aggregation in ionic liquid (IL) examined in TEM and SAXS experiments reveals the role of ionic interactions on the aggregation process. Lastly, we demonstrate that polymer grafted particles with ionic ends, and their resultant structures in ionic liquid enable significant improvement in their conductivity. The new copolymer-grafted iron oxide nanoparticles offer promising uses in electroactive actuators and ion-conducting membranes.

EXPERIMENTAL SECTION

Materials. 2,2'-Azobis(isobutyronitrile) (AIBN, 98%) was recrystallized from methanol. 1-Hexyl-3-methylimidazolium bis(trifluoromethylsulfonyl)imide, [HMIM][TFSI] (98%), sodium 4-vinylbenzenesulfonate (90%), trioctylamine (98%), butylamine (99.5%), and dimethylacetamide (DMAc, 99%) were purchased from Sigma-Aldrich and used as received. Toluene (HPLC grade), methanol (ACS grade), and hydrochloric acid (ACS grade) were purchased from Pharmco-AAPER. Oleic acid and oleylamine-stabilized Fe_3O_4 nanoparticles were synthesized by a high-temperature thermal decomposition method.³³

Characterization of PS-*b*-PSSTOA-Grafted Fe_3O_4 Nanoparticles. Copolymer-grafted Fe_3O_4 nanoparticles were ground mixed with KBr powder and then pressed into pellets for testing in Bruker Optics Tensor 27 FTIR spectrometer. Spectra were recorded for wavenumbers between 4000 and 400 cm^{-1} . Size distribution of polymer-grafted Fe_3O_4 nanoparticles was measured by dynamic light scattering (DLS) with a Malvern Zetasizer NanoS.

Film Preparation and Characterization. Poly(styrene-*b*-trioctylammonium *p*-styrenesulfonate)-grafted Fe_3O_4 nanoparticles in toluene (10 mg/mL) were mixed with a prescribed amount of ionic liquid and then bath-sonicated. A trace amount of DMAc was added to improve the miscibility of the ionic liquid with toluene. 50 mL of particle solution was cast on a 10 mm × 8 mm Kapton film at room temperature to prepare films of particles. SAXS experiments were performed directly on samples on Kapton. SAXS measurements were conducted at Beamline X27C at the National Synchrotron Light Source (NSLS), Brookhaven National Laboratory. The incident beam wavelength (λ) was 1.371 Å, monochromatized using a double-multilayer (silicon/tungsten) monochromator. Radial integration of the scattering intensity was rendered using Polar software (Stonybrook

Technology and Applied Research (STAR), Inc., Stony Brook, NY). The angular position of the SAXS patterns was calibrated using a silver behenate standard. Scattering of Kapton film was also collected as a background pattern and subtracted for each sample as follows: $\{\text{Corrected Scattering Pattern}\} = \{\text{Sample Pattern}\}/I_1(\text{sample}) - T\{\text{Background Pattern}\}/I_1(\text{background})$, where T is the transmission ratio and I_1 is the measured beam intensity. The scattering data are analyzed using the Igor Macros package developed by the NIST Center for Neutron Research^{34,35} and the unified fit of Irena package.³⁶

Conductivity tests were run on films on Kapton substrates at room temperature using a four-point probe with a digital multimeter (model 2000, Keithley Instruments Inc.). Conductivity (σ_0) of the films was calculated by $\sigma_0 = l/R_e A$, where l is the distance between electrodes, R_e is the measured film resistance, and A is the film area normal to ion flux.

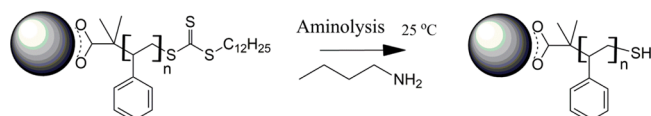
Transmission Electron Microscopy and Tomography. Particle aggregation was examined in transmission electron microscopy (FEI CM20 FE S/TEM) operated at 200 keV. TEM samples were prepared by drop-casting on a Formvar-coated copper grid. Tomography tilt series were acquired by bright-field imaging using a JEOL 1400 TEM operating at an accelerating voltage of 120 kV. Images were recorded with tilt angles ranging from -64° to $+64^\circ$. Alignment and reconstruction were performed using IMOD software package (University of Colorado).³⁷ Alignment of the tilt series was achieved with the seed-tracking procedure. 10–15 nanoparticles were chosen manually as seeds and were tracked automatically over the entire tilt series for alignment.

RESULTS AND DISCUSSION

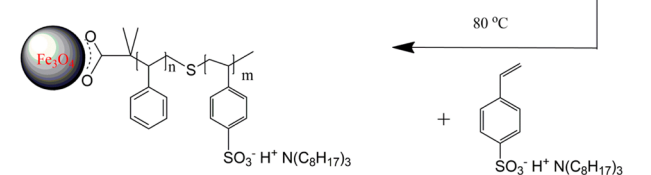
Preparation of Poly(styrene-*b*-styrenesulfonate) (PS-*b*-PSS) Grafted Nanoparticles. Scheme 1 outlines the synthetic route of functionalizing Fe_3O_4 nanoparticles with PS-*b*-PSS block copolymers. The first step is to graft PS chains onto ~ 6 nm Fe_3O_4 nanoparticles in diameter. 100 kg/mol PS (PDI: 1.07) was prepared by reversible addition–fragmentation chain transfer (RAFT) polymerization with 2-(((dodecylsulfanyl)carbonothioyl)sulfanyl)propanoic acid (DCSPA) as a chain transfer agent (CTA).^{38,39} Resultant polymers were

Scheme 1. Reaction Scheme of PS_n -*b*-PSSTOA_m Copolymer Grafted Fe_3O_4 Nanoparticles

Step 1



Step 2



capped with a carboxyl group (R group of CTA) at one end and a trithiocarbonate (Z group of CTA) on another. Carboxyl group functionalized PS chains were immobilized onto Fe_3O_4 surfaces through a ligand exchange reaction.²⁷

Preparation of Grafted PS with Thiol Terminus. Trithiocarbonate termini of 100 kg/mol PS grafted chains were converted to thiol groups by aminolysis⁴⁰ with butylamine as depicted in Scheme 1. A dilute solution (1 mg/mL) of PS-

grafted nanoparticles in toluene was degassed with three cycles of freeze–pump–thaw. Butylamine (50-fold in excess) was added to the solution of grafted nanoparticles under a flow of nitrogen and mixed for 24 h at room temperature. Particles were then precipitated with hexane or ethanol three times and redissolved in toluene. FTIR analyses before and after aminolysis are shown in Figure 1a. Spectra are normalized

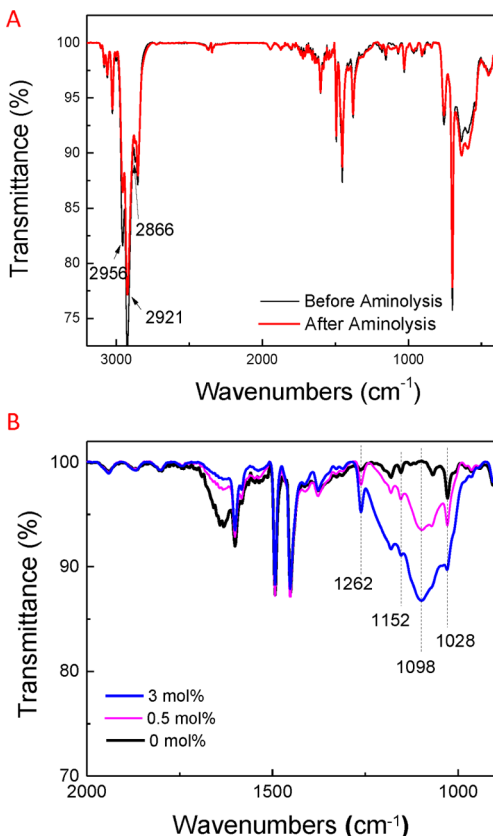


Figure 1. FTIR spectra of (A) PS-grafted Fe_3O_4 nanoparticles before (black) and after (red) aminolysis and (B) PS-*b*-PSS-grafted Fe_3O_4 nanoparticles. Spectra are normalized to the peak height of the aromatic combination bands at 2000–1660 cm^{-1} . All particles have graft density of 0.059 chains/ nm^2 .

with the aromatic C–H stretches at 3081 and 3025 cm^{-1} and combination bands at 2000–1630 cm^{-1} . C–S and C–S–H stretching vibrations give rise to very weak IR absorptions.⁴¹ It is observed that methyl C–H symmetric and asymmetric stretches at 2956 and 2866 cm^{-1} and methylene C–H symmetric stretch at 2921 cm^{-1} decrease with the addition of thiol groups.

PS-*b*-PSSTOA was prepared by adding alkene moieties of trioctylammonium (SSTOA) to thiolated PS via radical thiol–ene reaction⁴² in the presence of azobis(isobutyronitrile) (AIBN) as the thermal radical initiator. SSTOA was prepared according to reported procedures^{43,44} and verified by FTIR analysis (Figure S1). PS-grafted nanoparticles with thiol termini (SH), AIBN, and SSTOA were dissolved in toluene and degassed with freeze–pump–thaw. The molar ratio of [SH]:[AIBN] was kept as 1:0.5, and [SH]:[SSTOA] was varied to control the amount of SSTOA per PS chain (Table 1). Reaction was carried out at 80 °C for 4 h under nitrogen. Particles were precipitated in ethanol three times and redissolved in toluene.

Table 1. Synthetic Parameters for PS-*b*-PSSTOA-Grafted Fe_3O_4 Nanoparticles

graft density (chains/ nm^2)	[SH]:[AIBN]	[AIBN]:[SSTOA]	theoretical SS amount (mol %, SP)	no. of ions per particle
0.016	1:2	2:1	0.1	3
0.059	1:0.5	1:1	0.05	5
0.059	1:0.5	1:10	0.5	50
0.059	1:0.5	1:30	1.5	150
0.059	1:0.5	1:60	3	300
0.059	1:0.5	1:120	6	600

The radical thiol–ene reaction mechanism is similar to a chain transfer polymerization consisting of initiation, propagation, chain transfer to other thiols, and radical–radical termination steps (Scheme S1).^{42,45} In our experiments, thiyl radicals are formed via hydrogen abstraction from thiols to free radicals generated by thermal decomposition of AIBN initiator in solution. When an SS monomer adds to a thiyl radical, a benzylic radical is formed and the propagation rate exceeds that of chain transfer,⁴⁶ allowing chains to propagate. By varying the molar ratio of SS to thiols, different sulfonate composition is achieved. The possibility of termination between radicals is negligible because of the low graft density of chains in dilute solutions.

We performed FTIR measurements to identify the grafted SSTOA-PS and SS content. Absorption spectra of Fe_3O_4 nanoparticles with graft density of 0.059 chains/ nm^2 are shown in Figure 1b. Spectra are normalized to the peak height of the aromatic combination bands at 2000–1660 cm^{-1} . The asymmetric stretches of SO₃⁻ at 1098 and 1028 cm^{-1} increase as more SS is added to PS chains. Interestingly, at very low sulfonation percentage (SP) (0.05 mol %), the asymmetric stretches of SO₃⁻ are larger (Figure S2a,b) than the other samples. The asymmetric stretching vibration and the band splitting are primarily due to the effect of electrostatic field of the cation.⁴⁷ At very low SP, the interaction of a cation with its neighbor anion is negligible. As SP increases, the effective electrostatic field diminishes by the neighboring anions, which may lead to the smaller and broader band. The ¹H NMR spectrum on ungrafted PS-*b*-PSS in d-chloroform was also run to determine SP values; however, the peak of the H in methyl groups of TOA at 0.88 ppm (Figure S2c) was too small to conclude on the sulfonic amount of different samples.

In a medium with low dielectric constant, such as toluene or PS, ionic groups tend to form clusters due to strong ionic interactions.⁴⁸ Hydrodynamic cluster sizes of copolymer-grafted particles in toluene are determined using dynamic light scattering (DLS). Figure 2 shows that hydrodynamic diameter of clusters increases with the amount of sulfonate groups in copolymer grafts arising from strong ionic interactions. It is worth noting that all copolymer-grafted nanoparticles agglomerate over time, but they can be redispersed in toluene after sonication (Figure S3). The aggregation of TOA protected sulfonic groups is unlike what has been reported by Weiss et al.,⁴⁹ where trioctylammonium was used to shield ionic interactions which in turn reduced the glass-transition temperature with an increase in sulfonation fraction of PS.

Next, we examined the effect of ionic interactions on organization of PS-*b*-PSSTOA copolymer-grafted nanoparticles in TEM. Films of particles were prepared by solution-casting on a copper grid for TEM analysis. Particles with graft density of 0.016 chains/ nm^2 form strings (Figure 3a), which was reported

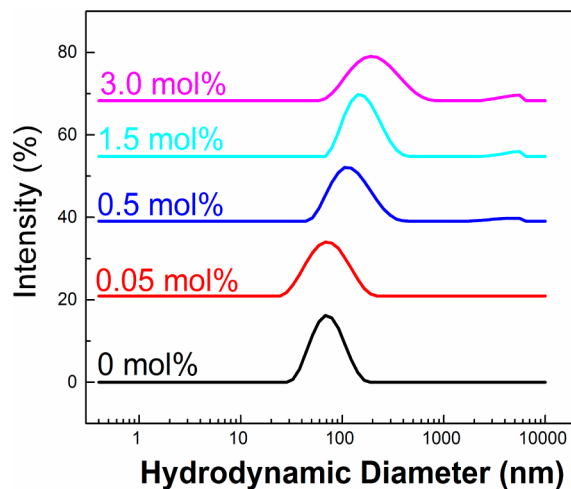


Figure 2. DLS of PS-*b*-PSSTOA grafted Fe_3O_4 nanoparticles at different molar sulfonation percentages (SP). Curves are shifted vertically. Graft density is 0.059 chains/ nm^2 .

in our previous work,¹⁷ TEM micrographs of PS-*b*-PSSTOA grafted particles (at 0.1 mol % SP, corresponds to ~3 ion pairs per particle) show that strings are close-packed and form monolayer-like aggregates (Figure 3b). We performed transmission electron tomography experiments to better understand the planar-like organization of particles. Orthogonal slices of the corresponding tomography reconstruction volume clearly reveal that particles organize into a plane with a single-particle thickness (Figure 3c). We sketch a postulated morphology in Figure 3e, where grafted chains are conformed around the connected strings in a sheet-like morphology. This planar structure is driven by particle–particle interactions combined with the immiscibility of ionic ends with long hydrophobic chains. We further conducted SAXS experiments on particles cast on a Kapton film. The repulsion peak in SAXS data, which appears at 0.2 nm^{-1} in pure PS-grafted particles, is no longer seen, and the slope at low q indicates the aggregates are surface fractals (Figure 3d).

By using particles with higher graft density (0.059 chains/ nm^2), the number of ions per particle is increased. Figure 4 shows that with the increment of ions per particle (see Table 1) string forming particles are connected side-by-side at 0.05 mol

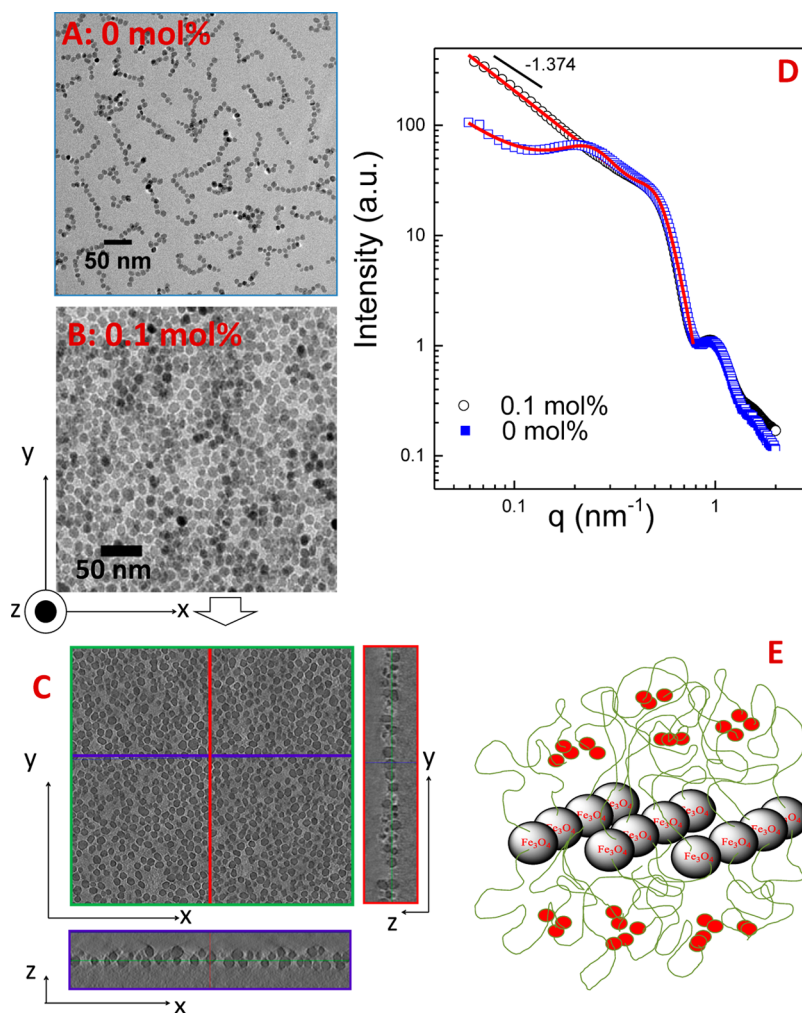


Figure 3. (A, B) TEM micrographs of PS-grafted (0 mol %) and PS-*b*-PSSTOA grafted (0.1 mol % SP) Fe_3O_4 nanoparticles. (C) TEM tomography images represent the orthogonal slices of the tomographic volume for sample with 0.1 mol % SP. (D) SAXS profiles of corresponding particles cast on Kapton films. Red lines are scattering fittings. Particles have graft density of 0.016 chains/ nm^2 . (E) Cartoon shows the arrangements of grafted chains as particle strings form compact side-by-side aggregates. Sulfonic units of the copolymer-grafted chains are shown in red circles.

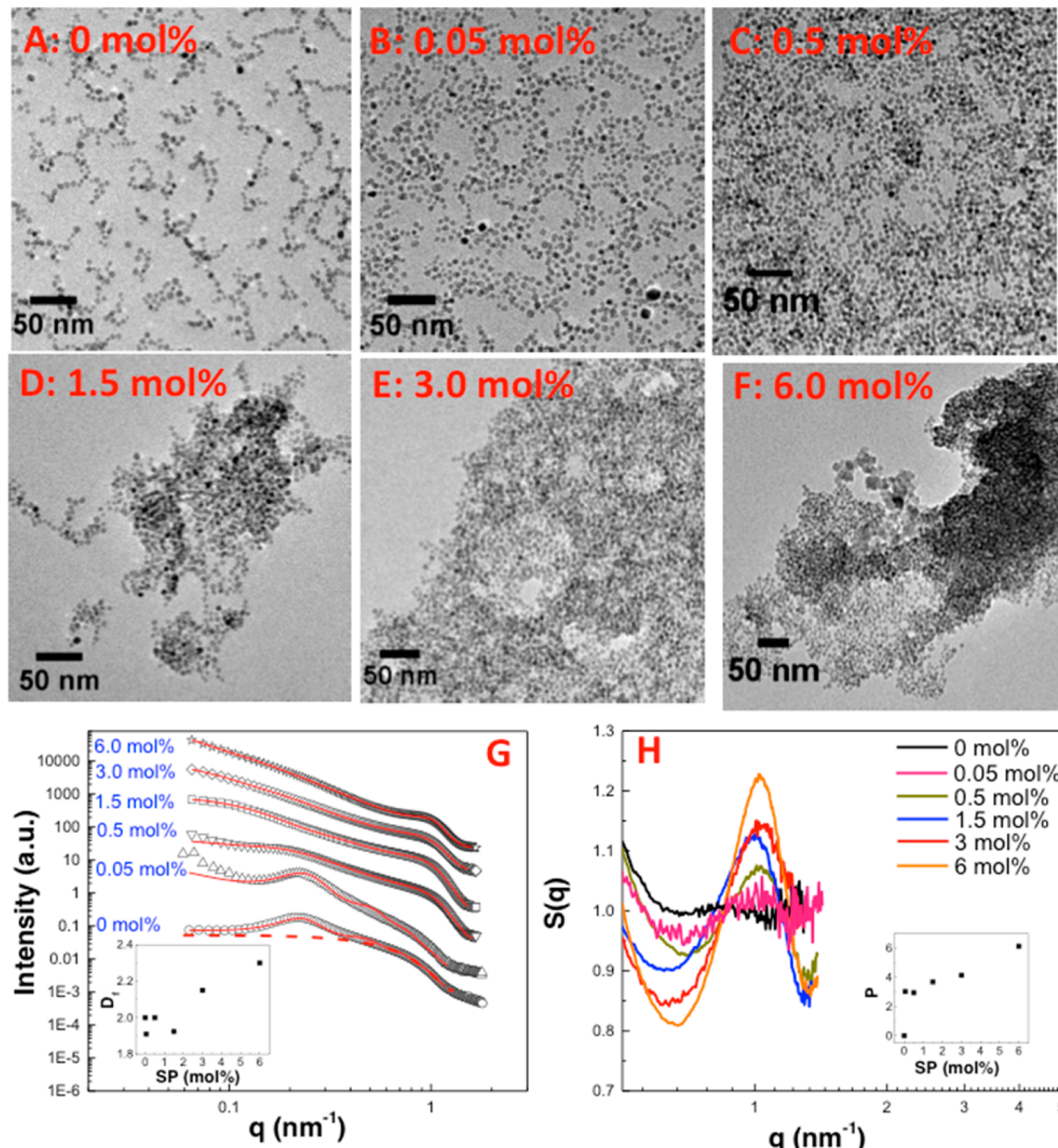


Figure 4. (A–F) TEM micrographs of PS-grafted nanoparticles with 0, 0.05, 0.5, 1.5, 3.0, and 6 mol % SP. Particles have grafting density of 0.059 chains/ nm^2 . (G) SAXS profiles of nanoparticles at different SP. Red lines are scattering fittings. The dashed line is the representative spherical form factor used to fit the data. Fractal dimension (D_f) increases with SP as shown in the inset. (H) Structure factor, $S(q)$, at high q shows the effect of sulfonation degree on the correlation degree of particles. Inset is the packing parameter (P) vs SP mol %.

% and then aggregate into close-packed particles at 0.5 mol % (Figures 4b,c). At 6 mol % SP, particles are strongly aggregated (Figure 4f). To gain information on the internal structure of the clusters, we ran our particles in SAXS. While TEM and SAXS represent the aggregation of particles in thin films and micron thick films, respectively, both techniques provide a good insight on the way particles aggregate with the ionic groups. Scattering data are first fit to a polydisperse sphere form factor,⁵⁰ $P(q)$. Structure factor, $S(q)$, is obtained by dividing $I(q)$ by $P(q)$. At high q , a correlation peak increases with the ion content (Figure 4h). This region is analyzed by fitting a structure factor function based on Born–Green approximation⁵¹ $S_{\text{BG}}(q) = 1/(1 +$

$P\Phi(q,d))$. P is the packing factor and equals to $8v_0/v_1$, where v_0 is the a spherical particle volume and v_1 is the volume available per particle. $\Phi(q,d)$ is defined as $\Phi(q,d) = 3[(\sin(qd) - qd \cos(qd))/(qd)^3]$. This analysis allows us to find the nearest packing of particles. Average distance between the spatially correlated particles is represented by d , which is found to be close to the average diameter of nanoparticles in all samples from the fittings. The packing factor increases as the number of incorporated ions per particle increases (see inset in Figure 4h). In 0, 0.05, and 0.5 mol % samples with a repulsive low- q peak, the Percus–Yevick potential was applied for the correlated spherical particles. Therefore, $I(q)$ is expressed as $I(q) =$

$P_{\text{polysphere}}(q)S_{\text{fractal}}(q)S_{\text{PY}}(q)$. The fractal structure factor, S_{fractal} , was used to fit the low- q data. S_{fractal} is defined as⁵² $S_{\text{fractal}}(q) = 1 + [\sin[(D_f - 1) \tan^{-1}(q\xi)]]/(qR_{\text{avg}})^{D_f}][(D_f \Gamma(D_f - 1))/(1 + (1/(q^2 \xi^2))^{(D_f-1)/2})]$, where D_f is the fractal dimension, ξ is the correlation length, and Γ is the gamma function. S_{PY} is the Percus–Yevick potentials for intercluster structure correlations, and $P_{\text{polysphere}}$ is the sphere form factor with Gaussian size distribution (see Supporting Information for $P_{\text{polysphere}}$).²⁹ The increase of D_f with sulfonation amount verifies the clustering observed in their TEM images.

In summary, we have discussed the sulfonation amount effect on particle aggregation in Figures 3 and 4. These samples enable us to further comment on the steric repulsion and electrostatic effect of sulfonated particles. If we compare the particles with different graft densities but similar number of ions per particle, which are the first two samples with 0.016 and 0.059 chains/nm² graft densities in Table 1, strings connected side-by-side are apparent in both systems (Figures 3b and 4b). However, there is clear discrepancy between the two structures. While particles with 0.016 chains/nm² are close-packed planar-like objects (Figure 3b), particles with 0.059 chains/nm² density form fishnet-like structures (Figure 4b). The steric repulsion from the higher density grafted PS chains prevents the close-packed aggregation of particles. This is also represented with the repulsion peak in SAXS data, indicating an average spacing between the particles (Figure 4g). With the discussion of samples in Figure 4, it becomes clear that the electrostatic effect dominates the steric repulsion of grafts for particles with increasing sulfonation amounts at the same graft density.

Organization of Copolymer-Grafted Fe₃O₄ Nanoparticles in Ionic Liquids (IL). Incorporation of ILs into block copolymers has been widely studied to understand their effect on the phase behavior of diblock copolymers and hence ion conductivity.^{53–56} The ion transport mechanism has been explained with the formation and breaking of ionic bonds between sulfonate groups and cations of IL as well as the vehicular diffusion of IL along the PSS domain.⁵⁷ It was shown that the effective segregation strength of a block copolymer increased with ionic liquid addition.⁵⁸ Likewise, interactions between IL and polystyrene-grafted nanoparticles with sulfonic ends can influence the solubility and aggregation states of particles. In this work, 1-hexyl-3-methylimidazolium bis-(trifluoromethylsulfonyl)imide, [HMIM][TFSI], is chosen among different types of ionic liquids due to its hydrophobic nature and chemical stability in air. Hildebrand solubility parameters of [HMIM][TFSI], toluene, and PS are known as 20.2, 18.0, and 18.65 MPa^{0.5} at 25 °C, respectively.^{59,60} A small amount of dimethylacetamide (DMAc, 0.1–3 vol %) was added to improve the miscibility of [HMIM][TFSI] with toluene. TEM images of particles in Figure 5 indicate that particle aggregations at different sulfonation amounts do not change in IL. SAXS profiles confirm that aggregation is not disrupted with IL addition, and similar fractal dimensions are obtained (inset in Figure 5d) as seen in particles without IL. The tomographic image of 3 mol % sample shows the aggregated structures of 5–6 particles thick through the sample thickness (Figure 5c). TEM images of the x - y planes of orthogonal slices Z1, Z2, and Z3—which are apart from each other by more than a particle size—exhibit several monolayers of particles, suggesting that planar clusters are stacked in the z direction of thickness.

The in-plane conductivity measurements on samples show that conductivity of IL improves with the addition of particles

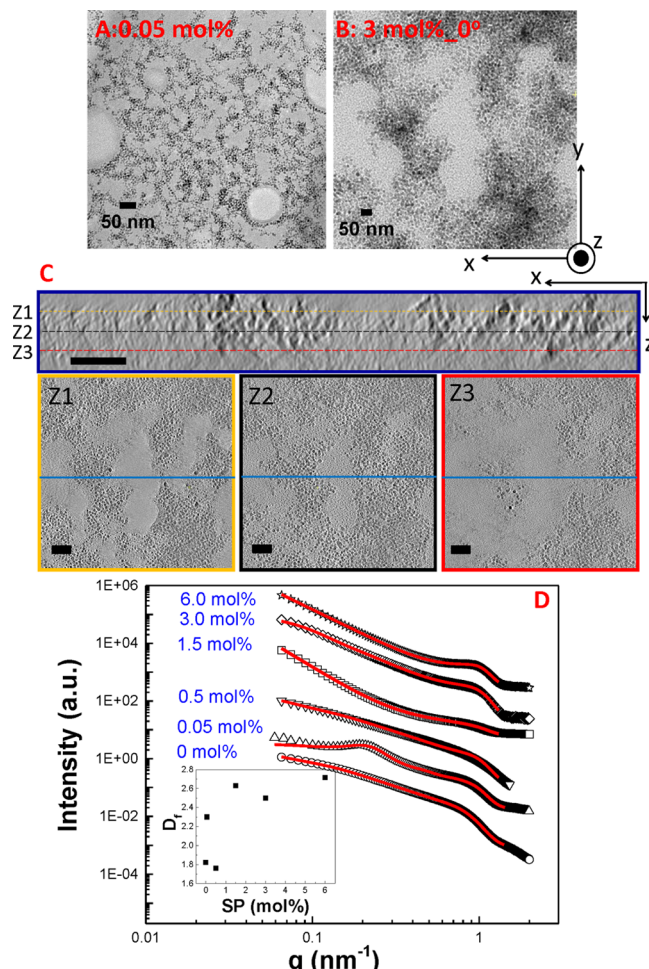


Figure 5. (A, B) TEM images display the aggregation of PS-*b*-PSSTOA-grafted Fe₃O₄ nanoparticles at 0.05 and 3 mol % SP in IL (30 wt %). (C) Orthogonal slices are shown in Z1, Z2, and Z3 of the tomographic volume for 3 mol % SP sample. Scale bars are 50 nm. (D) SAXS profiles of copolymer-grafted particles with varying SP in 30 wt % IL. The inset shows fractal dimension vs SP mol %.

up to 3 mol % sulfonation (Figure 6). We compare the conductivity values of our samples with two other systems containing high sulfonation levels: PSS-*b*-PMB block copolymer with sulfonation level of 17 mol % in [2-E-4-Mim]-[TFSI]⁵⁷ and 40 mol % in Nafion with [EMI][BF₄].⁶¹ We note that conductivity increases as SP changes from 0.05 to 3 mol %, and these values are interestingly close to or larger than the conductivity of Nafion with IL. We conclude that the higher conductivity value of 3 mol % sample is due to the planar-like aggregation of particles which are swollen with IL. Conductivity value of 6 mol % drops because of the strong aggregate heterogeneities in the sample (see Figure S4).

CONCLUSION

We have designed a new conductive system of polymer-grafted nanoparticles with charged groups in free ends of chains and demonstrated that conduction enhances with the aggregation state of our particles. Ion-containing block copolymer (PS-*b*-PSSTOA) grafted Fe₃O₄ nanoparticles with varying low (0.05–6 mol %) sulfonic amounts are prepared. The conductive solid films of particles are characterized using TEM tomography and SAXS. Magnetite particles with nonionic polymer chains

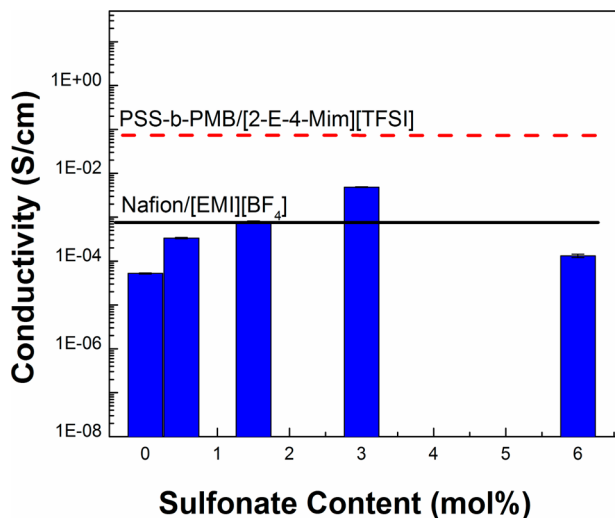


Figure 6. Conductivity of PS-*b*-PSS-grafted Fe_3O_4 nanoparticles with 0, 0.05, 1.5, 3, and 6 mol % SP in 30 wt % IL loading. Black solid and red dashed lines represent the room-temperature conductivity values of Nafion with $[\text{EMI}][\text{BF}_4]$ (50 wt % IL) (from ref 61) and PSS-*b*-PMB copolymer with $[2\text{-E-4-Mim}][\text{TFSI}]$ (71 wt % IL) (from ref 57), respectively. Particles have grafting density of 0.059 chains/ nm^2 .

present well-ordered strings in both bulk and thin films. With sulfonic group coordination to the ends of grafted chains, copolymer grafted nanoparticles form compact, sheet-like networks in the ionic liquid (IL). TEM tomography results substantiate this aggregation which becomes possible through interchain cross-linking of ionic units in the grafted chains. These functionalized nanoparticles are proposed to enhance conductivity with the pathways created between planar-like clusters.

ASSOCIATED CONTENT

Supporting Information

Schema of radical thiol–ene click reaction; FTIR spectra of TOA, SS, and SSTOA; FTIR spectra of PS-*b*-PSS grafted Fe_3O_4 nanoparticles with graft density of 0.016 chains/ nm^2 ; stability of particles in toluene; TEM of PS-*b*-PSS-grafted Fe_3O_4 nanoparticles with 6 mol % SP. The Supporting Information is available free of charge on the ACS Publications website at DOI: 10.1021/acs.macromol.5b00758.

AUTHOR INFORMATION

Corresponding Author

*E-mail pakcora@stevens.edu (P.A.).

Notes

The authors declare no competing financial interest.

ACKNOWLEDGMENTS

We acknowledge financial support from NSF-DMR CAREER grant (#1048865) and REU Supplement (#1235775). Portions of this work were performed at Beamline X27C at the National Synchrotron Light Source (NSLS), Brookhaven National Laboratory. NSLS is supported by the U.S. Department of Energy, Office of Science, Office of Basic Energy Sciences, under Contract DE-AC02-98CH10886. Research carried out in part at the Center for Functional Nanomaterials (CFN), Brookhaven National Laboratory, which is supported by the U.S. Department of Energy, Office of Basic Energy Sciences,

under Contract DE-SC0012704. We thank Dr. Huolin Xin for his help with TEM tomography at CFN.

REFERENCES

- (1) Lu, Y.; Das, S. K.; Moganty, S. S.; Archer, L. A. Ionic liquid-nanoparticle hybrid electrolytes and their application in secondary lithium-metal batteries. *Adv. Mater.* **2012**, *24* (32), 4430–4435.
- (2) Croce, F.; Appetecchi, G. B.; Persi, L.; Scrosati, B. Nano-composite polymer electrolytes for lithium batteries. *Nature* **1998**, *394* (6692), 456–458.
- (3) Vargantwar, P. H.; Roskov, K. E.; Ghosh, T. K.; Spontak, R. J. Enhanced biomimetic performance of ionic polymer-metal composite actuators prepared with nanostructured block ionomers. *Macromol. Rapid Commun.* **2012**, *33* (1), 61–68.
- (4) Wang, X. L.; Oh, I. K.; Kim, J. B. Enhanced electromechanical performance of carbon nano-fiber reinforced sulfonated poly(styrene-*b*-[ethylene/butylene]-*b*-styrene) actuator. *Compos. Sci. Technol.* **2009**, *69* (13), 2098–2101.
- (5) Lu, Y.; Moganty, S. S.; Schaefer, J. L.; Archer, L. A. Ionic liquid-nanoparticle hybrid electrolytes. *J. Mater. Chem.* **2012**, *22* (9), 4066–4072.
- (6) Walls, H. J.; Riley, M. W.; Singhal, R. R.; Spontak, R. J.; Fedkiw, P. S.; Khan, S. A. Nanocomposite electrolytes with fumed silica and hectorite clay networks: Passive versus active fillers. *Adv. Funct. Mater.* **2003**, *13* (9), 710–717.
- (7) Nordstrom, J.; Matic, A.; Sun, J.; Forsyth, M.; MacFarlane, D. R. Aggregation, ageing and transport properties of surface modified fumed silica dispersions. *Soft Matter* **2010**, *6* (10), 2293–2299.
- (8) Choi, N.-S.; Lee, Y. M.; Lee, B. H.; Lee, J. A.; Park, J.-K. Nanocomposite single ion conductor based on organic–inorganic hybrid. *Solid State Ionics* **2004**, *167* (3–4), 293–299.
- (9) Ju, S. H.; Lee, Y.-S.; Sun, Y.-K.; Kim, D.-W. Unique core-shell structured $\text{SiO}_2(\text{Li}^+)$ nanoparticles for high-performance composite polymer electrolytes. *J. Mater. Chem. A* **2013**, *1* (2), 395–401.
- (10) Lee, Y.-S.; Ju, S. H.; Kim, J.-H.; Hwang, S. S.; Choi, J.-M.; Sun, Y.-K.; Kim, H.; Scrosati, B.; Kim, D.-W. Composite gel polymer electrolytes containing core-shell structured $\text{SiO}_2(\text{Li}^+)$ particles for lithium-ion polymer batteries. *Electrochim. Commun.* **2012**, *17* (0), 18–21.
- (11) Nugent, J. L.; Moganty, S. S.; Archer, L. A. Nanoscale Organic Hybrid Electrolytes. *Adv. Mater.* **2010**, *22* (33), 3677–3680.
- (12) Wen, Y. H.; Lu, Y.; Dobosz, K. M.; Archer, L. A. Structure, ion transport, and rheology of nanoparticle salts. *Macromolecules* **2014**, *47* (13), 4479–4492.
- (13) Sato, T.; Morinaga, T.; Marukane, S.; Narutomi, T.; Igarashi, T.; Kawano, Y.; Ohno, K.; Fukuda, T.; Tsujii, Y. Novel solid-state polymer electrolyte of colloidal crystal decorated with ionic-liquid polymer brush. *Adv. Mater.* **2011**, *23* (42), 4868–4872.
- (14) Akcora, P.; Liu, H.; Kumar, S. K.; Moll, J.; Li, Y.; Benicewicz, B. C.; Schadler, L. S.; Acehan, D.; Panagiotopoulos, A. Z.; Pryamitsyn, V.; Ganeshan, V.; Ilavsky, J.; Thiagarajan, P.; Colby, R. H.; Douglas, J. F. Anisotropic self-assembly of spherical polymer-grafted nanoparticles. *Nat. Mater.* **2009**, *8* (4), 354–359.
- (15) Green, P. F. The structure of chain end-grafted nanoparticle/homopolymer nanocomposites. *Soft Matter* **2011**, *7* (18), 7914–7926.
- (16) Kumar, S. K.; Jouault, N.; Benicewicz, B.; Neely, T. Nanocomposites with polymer grafted nanoparticles. *Macromolecules* **2013**, *46* (9), 3199–3214.
- (17) Pryamitsyn, V.; Ganeshan, V.; Panagiotopoulos, A. Z.; Liu, H.; Kumar, S. K., Modeling the anisotropic self-assembly of spherical polymer-grafted nanoparticles. *J. Chem. Phys.* **2009**, *131* (22).22110210.1063/1.3267729.
- (18) Fernandes, N. J.; Koerner, H.; Giannelis, E. P.; Vaia, R. A. Hairy nanoparticle assemblies as one-component functional polymer nanocomposites: Opportunities and challenges. *MRS Commun.* **2013**, *3* (1), 13–29.
- (19) Estridge, C. E.; Jayaraman, A., Assembly of diblock copolymer functionalized spherical nanoparticles as a function of copolymer

- composition. *J. Chem. Phys.* **2014**, *140* (14), 14490510.1063/1.4870592.
- (20) Ginzburg, V. V. Polymer-grafted nanoparticles in polymer melts: Modeling using the combined scft-dft approach. *Macromolecules* **2013**, *46* (24), 9798–9805.
- (21) Jayaraman, A. Polymer grafted nanoparticles: Effect of chemical and physical heterogeneity in polymer grafts on particle assembly and dispersion. *J. Polym. Sci., Part B: Polym. Phys.* **2013**, *51* (7), 524–534.
- (22) Koerner, H.; Drummy, L. F.; Benicewicz, B.; Li, Y.; Vaia, R. A. Nonisotropic self-organization of single-component hairy nanoparticle assemblies. *ACS Macro Lett.* **2013**, *2* (8), 670–676.
- (23) Rungra, A.; Natarajan, B.; Neely, T.; Dukes, D.; Schadler, L. S.; Benicewicz, B. C. Grafting bimodal polymer brushes on nanoparticles using controlled radical polymerization. *Macromolecules* **2012**, *45* (23), 9303–9311.
- (24) Vogiatzis, G. G.; Theodorou, D. N. Structure of polymer layers grafted to nanoparticles in silica-polystyrene nanocomposites. *Macromolecules* **2013**, *46* (11), 4670–4683.
- (25) Nair, N.; Jayaraman, A. Self-consistent PRISM theory-Monte Carlo simulation studies of copolymer grafted nanoparticles in a homopolymer matrix. *Macromolecules* **2010**, *43* (19), 8251–8263.
- (26) Zhu, X.; Wang, L.; Lin, J.; Zhang, L. Ordered nanostructures self-assembled from block copolymer tethered nanoparticles. *ACS Nano* **2010**, *4* (9), 4979–4988.
- (27) Jiao, Y.; Akcora, P. Assembly of polymer-grafted magnetic nanoparticles in polymer melts. *Macromolecules* **2012**, *45* (8), 3463–3470.
- (28) Senses, E.; Jiao, Y.; Akcora, P. Modulating interfacial attraction of polymer-grafted nanoparticles in melts under shear. *Soft Matter* **2014**, *10* (25), 4464–4470.
- (29) Jiao, Y.; Akcora, P. Understanding the role of grafted polystyrene chain conformation in assembly of magnetic nanoparticles. *Phys. Rev. E* **2014**, *90* (4), 042601.
- (30) Raman, V.; Sharma, R.; Hatton, T. A.; Olsen, B. D. Magnetic field induced morphological transitions in block copolymer/superparamagnetic nanoparticle composites. *ACS Macro Lett.* **2013**, *2* (8), 655–659.
- (31) Xu, C.; Ohno, K.; Ladmiral, V.; Composto, R. J. Dispersion of polymer-grafted magnetic nanoparticles in homopolymers and block copolymers. *Polymer* **2008**, *49* (16), 3568–3577.
- (32) Jiao, Y.; Parra, J.; Akcora, P. Effect of Ionic Groups on Polymer-Grafted Magnetic Nanoparticle Assemblies. *Macromolecules* **2014**, *47* (6), 2030–2036.
- (33) Sun, S.; Zeng, H.; Robinson, D. B.; Raoux, S.; Rice, P. M.; Wang, S. X.; Li, G. Monodisperse MFe₂O₄ (M = Fe, Co, Mn) Nanoparticles. *J. Am. Chem. Soc.* **2004**, *126* (1), 273–279.
- (34) Kline, S. R. Reduction and analysis of SANS and USANS data using IGOR Pro. *J. Appl. Crystallogr.* **2006**, *39* (6), 895–900.
- (35) Lee, J. M.; Ok, H. K.; Sang, E. S.; Lee, B. H.; Choe, S. Reversible addition-fragmentation chain transfer (RAFT) bulk polymerization of styrene: Effect of R-group structures of carboxyl acid group functionalized RAFT agents. *Macromol. Res.* **2005**, *13* (3), 236–242.
- (36) Ilavsky, J.; Jemian, P. R. Irena: tool suite for modeling and analysis of small-angle scattering. *J. Appl. Crystallogr.* **2009**, *42* (2), 347–353.
- (37) Kremer, J. R.; Mastronarde, D. N.; McIntosh, J. R. Computer visualization of three-dimensional image data using IMOD. *J. Struct. Biol.* **1996**, *116* (1), 71–76.
- (38) Lai, J. T.; Filla, D.; Shea, R. Functional Polymers from Novel Carboxyl-Terminated Trithiocarbonates as Highly Efficient RAFT Agents. *Macromolecules* **2002**, *35* (18), 6754–6756.
- (39) Yang, Y.; Yang, Z.; Zhao, Q.; Cheng, X.; Tjong, S. C.; Li, R. K. Y.; Wang, X.; Xie, X. Immobilization of RAFT agents on silica nanoparticles utilizing an alternative functional group and subsequent surface-initiated RAFT polymerization. *J. Polym. Sci., Part A: Polym. Chem.* **2009**, *47* (2), 467–484.
- (40) Liu, Y.; Cavicchi, K. A. Reversible Addition Fragmentation Chain Transfer (RAFT) Polymerization with a Polymeric RAFT Agent Containing Multiple Trithiocarbonate Groups. *Macromol. Chem. Phys.* **2009**, *210* (19), 1647–1653.
- (41) Coates, J. Interpretation of infrared spectra, a practical approach. *Encyclopedia of Analytical Chemistry*; Wiley: New York, 2000.
- (42) Lowe, A. B. Thiol-ene “click” reactions and recent applications in polymer and materials synthesis. *Polym. Chem.* **2010**, *1* (1), 17–36.
- (43) Liu, Y.; Pollock, K. L.; Cavicchi, K. A. Synthesis of poly(trioctylammonium p-styrenesulfonate) homopolymers and block copolymers by RAFT polymerization. *Polymer* **2009**, *50* (26), 6212–6217.
- (44) Cavicchi, K. A. Synthesis and polymerization of substituted ammonium sulfonate monomers for advanced materials applications. *ACS Appl. Mater. Interfaces* **2012**, *4* (2), 518–526.
- (45) Koo, S. P. S.; Stamenović, M. M.; Prasath, R. A.; Inglis, A. J.; Du Prez, F. E.; Barner-Kowollik, C.; Van Camp, W.; Junkers, T. Limitations of radical thiol-ene reactions for polymer–polymer conjugation. *J. Polym. Sci., Part A: Polym. Chem.* **2010**, *48* (8), 1699–1713.
- (46) Hoyle, C. E.; Lee, T. Y.; Roper, T. Thiol-enes: Chemistry of the past with promise for the future. *J. Polym. Sci., Part A: Polym. Chem.* **2004**, *42* (21), 5301–5338.
- (47) Zundel, G. *Hydration and Intermolecular Interaction: Infrared Investigations with Polyelectrolyte Membranes*; Academic: New York, 1969.
- (48) Eisenberg, A. Clustering of Ions in Organic Polymers. A Theoretical Approach. *Macromolecules* **1970**, *3* (2), 147–154.
- (49) Weiss, R. A.; Agarwal, P. K.; Lundberg, R. D. Control of ionic interactions in sulfonated polystyrene ionomers by the use of alkyl-substituted ammonium counterions. *J. Appl. Polym. Sci.* **1984**, *29* (9), 2719–2734.
- (50) Percus, J. K.; Yevick, G. J. Analysis of classical statistical mechanics by means of collective coordinates. *Phys. Rev.* **1958**, *110* (1), 1.
- (51) Guinier, A.; Fournet, G.; Walker, C. B.; Yudowitch, K. L. *Small-Angle Scattering of X-rays*; Wiley: New York, 1955.
- (52) Teixeira, J. Small-angle scattering by fractal systems. *J. Appl. Crystallogr.* **1988**, *21* (6), 781–785.
- (53) Singh, B.; Sekhon, S. Ion conducting behaviour of polymer electrolytes containing ionic liquids. *Chem. Phys. Lett.* **2005**, *414* (1), 34–39.
- (54) Matsumoto, K.; Endo, T. Confinement of Ionic Liquid by Networked Polymers Based on Multifunctional Epoxy Resins. *Macromolecules* **2008**, *41* (19), 6981–6986.
- (55) Kim, S. Y.; Kim, S.; Park, M. J. Enhanced proton transport in nanostructured polymer electrolyte/ionic liquid membranes under water-free conditions. *Nat. Commun.* **2010**, *1*, 1.
- (56) Elabd, Y. A.; Hickner, M. A. Block copolymers for fuel cells. *Macromolecules* **2011**, *44* (1), 1–11.
- (57) Kim, O.; Kim, S. Y.; Ahn, H.; Kim, C. W.; Rhee, Y. M.; Park, M. J. Phase Behavior and Conductivity of Sulfonated Block Copolymers Containing Heterocyclic Diazole-Based Ionic Liquids. *Macromolecules* **2012**, *45* (21), 8702–8713.
- (58) Virgili, J. M.; Hoarfrost, M. L.; Segalman, R. A. Effect of an ionic liquid solvent on the phase behavior of block copolymers. *Macromolecules* **2010**, *43* (12), 5417–5423.
- (59) Marciak, A. The solubility parameters of ionic liquids. *Int. J. Mol. Sci.* **2010**, *11* (5), 1973–1990.
- (60) Letcher, T. M.; Marciak, A.; Marciak, M.; Domańska, U. Activity coefficients at infinite dilution measurements for organic solutes in the ionic liquid 1-hexyl-3-methyl-imidazolium bis (trifluoromethylsulfonyl)-imide using glc at T = (298.15, 313.15, and 333.15) K. *J. Chem. Thermodyn.* **2005**, *37* (12), 1327–1331.
- (61) Sekhon, S. S.; Park, J. S.; Baek, J. S.; Yim, S. D.; Yang, T. H.; Kim, C. S. Small-angle X-ray scattering study of water free fuel cell membranes containing ionic liquids. *Chem. Mater.* **2010**, *22* (3), 803–812.